

# ***In vivo* cerebrovascular measurement combining diffuse near-infrared absorption and correlation spectroscopies**

**Cecil Cheung<sup>1</sup>, Joseph P Culver<sup>1</sup>, Kasushi Takahashi<sup>2</sup>,  
Joel H Greenberg<sup>2</sup> and A G Yodh<sup>1</sup>**

<sup>1</sup> Department of Physics and Astronomy, University of Pennsylvania, Philadelphia, PA 19104, USA

<sup>2</sup> Cerebrovascular Research Center, Department of Neurology, University of Pennsylvania School of Medicine, Philadelphia, PA 19104, USA

Received 21 March 2001

Published 6 July 2001

Online at [stacks.iop.org/PMB/46/2053](http://stacks.iop.org/PMB/46/2053)

## **Abstract**

We combine two near-infrared diffuse optical techniques to study variations of blood flow, haemoglobin concentration, and blood oxygen saturation in the functioning rat brain. Diffuse correlation spectroscopy (or flowmetry) monitors changes in the cerebral blood flow, without the use of the principles of tracer clearance, by measuring the optical phase-shifts caused by moving blood cells. Near-infrared absorption spectroscopy concurrently measures tissue absorption at two wavelengths to determine haemoglobin concentration and blood oxygen saturation in this same tissue volume. This optical probe is non-invasive and was employed through the intact skull. The utility of the technique is demonstrated *in vivo* by measuring the temporal changes in the regional vascular dynamics of rat brain during hypercapnia. Temporal and spatial variations of cerebral blood flow, haemoglobin concentration and blood oxygen saturation during hypercapnia are compared with other measurements in the literature, and a quantitative analysis demonstrating the self-consistency of our combined observations of vascular response is presented.

(Some figures in this article are in colour only in the electronic version; see [www.iop.org](http://www.iop.org))

## **1. Introduction**

The vascular changes that accompany neuronal activity represent a critical and incompletely understood component of neurophysiology. Energy is required for cerebral functions, and its conversion into a useful form is facilitated by oxygen delivered to the brain through the cerebral vasculature. For example, it is been shown that local activation of the cerebral cortex triggers local changes in the cerebral blood flow (Greenberg *et al* 1979, Lou *et al* 1987, Dirnagl *et al* 1994). The vascular responses corresponding to these effects appear to be increased blood

flow speed (Mandeville *et al* 1999), and an initial decrease in the blood oxygenation (Malonek and Grinvald 1996).

A range of non-invasive techniques have been used to probe activation of the cerebral cortex. Electrical signals originating from the firing of neurons can be measured with electroencephalography (EEG), changes in local cerebral glucose utilization and local cerebral blood flow can be measured with positron emission tomography (PET) (Phelps and Mazziotta 1985), and changes in the concentration of deoxyhaemoglobin and adenosine triphosphate can be measured with magnetic resonance imaging (MRI) (Kwong *et al* 1992, Chance 1989). Some relatively more invasive methods for studying the brain include laser Doppler flowmetry (LDF) and confocal microscopy. Both of these methods are used to study near-surface (or near-probe) tissue volumes. LDF measures the blood flow speed and the number of moving blood cells (Shepherd and Öberg 1990). However, LDF is primarily a surface technique, and in order to make these measurements in brain tissue the skull must be thinned to achieve sufficient signal. Confocal microscopy has been used to image the cortical capillary bed and erythrocytes through a cranial window. In this case, blood flow is estimated by counting the number of blood cells flowing through a capillary per unit time (Villringer *et al* 1994). Finally, a number of other techniques have been applied to measure cerebral tissue oxygen. These include microelectrodes (Nair *et al* 1975), phosphorescence quenching by oxygen in the microvasculature (Wilson *et al* 1993), and near-infrared spectroscopy (NIRS). NIRS relies on the difference between the absorption spectra of oxyhaemoglobin and deoxyhaemoglobin to determine blood oxygenation (Danen *et al* 1998). Generally these methods provide complementary information about brain tissue, and no technique has emerged as a universal choice for experiments in neurophysiology.

In the present study, we combine diffuse photon correlation methods, originally used to study highly scattering complex fluids (Maret and Wolf 1987, Pine *et al* 1988, Boas *et al* 1995), with a near-infrared diffuse wave regional imager (Danen *et al* 1998) for haemoglobin spectroscopy. The instrument enables us to simultaneously measure regional blood perfusion, haemoglobin concentration and blood oxygen saturation in the same, deep tissue volume. This combination of tools has not been previously employed, and because of the increased information it provides about vascular response, we anticipate that the probe will be valuable for future research on the physiology of deep, highly scattering tissue.

In this paper we introduce the basic underlying theory of the instrument, demonstrate its use in a tissue phantom, and investigate its utility *in vivo* by examining the cerebrovascular response to hypercapnia in rats. In particular, we measure the magnitude of the increase in blood flow during hypercapnia while concurrently probing variations in haemoglobin concentration, blood oxygen saturation and the degree of vascular heterogeneity.

The next section provides a theoretical background about diffuse light and correlation transport, and the photon correlation method. A description of our near-infrared instrument is presented in section 3. The animal preparation and the experimental procedures are described in section 4, and in section 5 we discuss our measurements and their implications, followed by concluding remarks in section 6.

## 2. Theory

A turbid medium such as biological tissue is characterized by a reduced scattering coefficient  $\mu'_s$ , and an absorption coefficient  $\mu_a$ , which in general can depend on position and time. Physically, the reciprocal of  $\mu'_s$  is the photon random walk step, corresponding to the length travelled by a photon in the medium before its initial direction becomes randomized; the reciprocal of  $\mu_a$  is the absorption length, corresponding to the length scale over which a

photon travelling in the medium will be absorbed. For many conditions of practical interest the photon fluence rate  $\Phi(\vec{r}, t)$  satisfies a diffusion equation, i.e.

$$\left(-\frac{1}{3\mu'_s}\nabla^2 + \mu_a + \frac{1}{v}\frac{\partial}{\partial t}\right)\Phi(\vec{r}, t) = S(\vec{r}, t) \tag{1}$$

where  $S(\vec{r}, t)$  is the source light distribution and  $v$  is the speed of light in the medium. For point sources of the form  $S(\vec{r}, t) = S_0\delta(\vec{r} - \vec{r}_s)\exp(-i\omega t)$ , equation (1) simplifies to:

$$\left(-\frac{1}{3\mu'_s}\nabla^2 + \mu_a - \frac{i\omega}{v}\right)\Phi(\vec{r}) = S_0\delta(\vec{r} - \vec{r}_s) \tag{2}$$

with

$$\Phi(\vec{r}, t) = \Phi(\vec{r})\exp(-i\omega t).$$

$\Phi(\vec{r})$  is the spatial part of the so-called diffuse photon density wave (DPDW) (Yodh and Chance 1995).

In our experiments light is collected in remission, i.e. light sources and detectors are arranged in a plane parallel to the air/tissue surface, and are oriented to receive or emit light normal to the air/tissue interface. We will approximate the tissue and tissue phantom samples as semi-infinite. The solution for diffuse photon density waves in this geometry is obtained using an image source approach following Kienle and Patterson (1997). The complex DPDW solution is:

$$\Phi(\rho) = \frac{3\mu'_s S_0}{4\pi} \left( \frac{\exp(-kr_1)}{r_1} - \frac{\exp(-kr_2)}{r_2} \right) \tag{3}$$

where  $k^2 = 3\mu'_s(-i\omega/v + \mu_a)$ ,  $r_1 = \sqrt{\rho^2 + z_o^2}$  and  $r_2 = \sqrt{\rho^2 + (z_o + 2z_b)^2}$ .  $\rho$  is the distance from the source to detector measured along the sample surface,  $z_b$  is the distance above the tissue surface at which the fluence rate extrapolates to zero,  $z_o$  is the effective depth of the source. We use  $z_o = (\mu'_s + \mu_a)^{-1}$ . The value of  $z_b$  depends on the refraction indices of tissue and air (Haskell *et al* 1994). In our analysis, we take  $n_{\text{tissue}} = 1.35$  and  $n_{\text{air}} = 1.0$ , so that  $z_b = 1.76/\mu'_s$ .

Multidistance measurements of the phase and the amplitude of the diffuse photon density wave enable one to deduce the optical properties ( $\mu'_s$  and  $\mu_a$ ) of the medium by fitting the known analytical solution, equation (3), to the measurements. In the near-infrared region, the dominant chromophore in tissue is haemoglobin, and the absorption spectra of oxyhaemoglobin and deoxyhaemoglobin are different (Zijlstra *et al* 1991, Yodh and Chance 1995). Thus, determination of  $\mu_a$  at two different optical wavelengths (786 nm and 830 nm) provides information sufficient for calculation of the concentrations of oxyhaemoglobin and deoxyhaemoglobin if one assumes a water/lipids ratio. In this paper, we assume a 1/1 ratio of water/lipids, and subtract the corresponding background spectra from our absorption measurements. The blood oxygen saturation and total haemoglobin concentration are then easily computed (Boas 1996).

We determine the motional dynamics of the medium by measuring the time dependence of detected diffuse light intensity  $I(\vec{r}, t)$ , and then computing the (normalized) intensity autocorrelation function:

$$g_2(\vec{r}, \tau) \equiv \frac{\langle I(\vec{r}, t)I(\vec{r}, t + \tau) \rangle}{\langle I \rangle^2} \tag{4}$$

where  $\langle \dots \rangle$  denotes a time average. For ergodic systems, the diffuse light electric field autocorrelation function  $G_1(\vec{r}, \tau) \equiv \langle \vec{E}(\vec{r}, \tau) \cdot \vec{E}^*(\vec{r}, t + \tau) \rangle$  is derived using the Siegert relation (Berne and Pecora 1976):

$$g_2(\vec{r}, \tau) = 1 + \beta \frac{|G_1(\vec{r}, \tau)|^2}{\langle I \rangle^2}. \tag{5}$$

Here  $\beta$  is a numerical factor which depends on the detector geometry. We have recently shown (for a continuous light sources) that  $G_1(\vec{r}, \tau)$  also satisfies a diffusion equation, though the equation differs slightly from equation (2) (Boas *et al* 1995, Boas and Yodh 1997, Hackmeier *et al* 1997), i.e.

$$\left( -\frac{1}{3\mu'_s} \nabla^2 + \mu_a + \frac{1}{3} \alpha \mu'_s k_0^2 \langle \Delta r^2(\tau) \rangle \right) G_1(\vec{r}, \tau) = S(\vec{r}). \quad (6)$$

Here  $k_0$  is the wavenumber of light in the medium,  $\langle \Delta r^2(\tau) \rangle$  is the mean squared displacement of the scatterers in the turbid medium during a time interval  $\tau$  and  $\alpha$  represents the probability that a light scattering event is with a moving scatterer (e.g. a flowing blood cell).

Two models can be used to describe the dynamics of cerebral blood flow. The first model was used originally in colloidal suspensions where the dynamics is Brownian, and  $\langle \Delta r^2(\tau) \rangle = 6D_B\tau$  where  $D_B$  is the diffusion coefficient of the colloid (Maret and Wolf 1987, Pine *et al* 1988). The second model argues that in a capillary network, blood flow resembles a random flow, i.e. both the speed and direction of the flow at any point in space are random. In such cases (Nossal *et al* 1971, Bonner and Nossal 1981),  $\langle \Delta r^2(\tau) \rangle = \langle V^2 \rangle \tau^2$ , where  $\langle V^2 \rangle$  is the mean squared velocity of the scatterers. We have analysed our data with both models, but for reasons to be explained in section 5, we chose to parametrize our data using the Brownian diffusion model. Thus the effective blood flow speed is parametrized by the Brownian diffusion coefficient  $D_B$  which depends on the exponential decay rate of the measured correlation functions. It is further assumed that the measured relative changes of  $D_B$  are equal to the relative changes in blood speed, and that  $\alpha$  is proportional to the tissue blood volume fraction. With these assumptions, the relative change of  $\alpha D_B$  equals the relative change of the cerebral blood flow (CBF). Justification and discussion of these assumptions will be given in section 5. We introduce the term ‘diffuse correlation flowmetry’ to represent the correlation method described above.

Analytic solutions of equation (6) for a point light source with unit intensity impinging upon a semi-infinite medium are formally the same as for the diffuse photon density waves (Boas 1996), i.e.

$$G_1(\rho, \tau) = \frac{3\mu'_s}{4\pi} \left( \frac{\exp(-k_D r_1)}{r_1} - \frac{\exp(-k_D r_2)}{r_2} \right) \quad (7)$$

where  $k_D^2 = 3\mu'_s \mu_a + 6\mu'_s k_0^2 \alpha D_B \tau$ ;  $r_1$  and  $r_2$  were defined earlier. Thus the measurements of  $G_1$  can be fitted to yield  $\alpha D_B$ , using given values of  $\rho$ , and measured values of  $\mu'_s$ ,  $\mu_a$  from concurrent DPDW measurements.

### 3. Instrument

Figure 1 shows a schematic diagram of the instrument. The sources of near-infrared (NIR) light were: (a) a single mode laser source with a coherence length ( $>1$  m) much longer than a typical photon path length, for the diffuse correlation flowmetry measurements and (b) two intensity modulated laser diodes for the diffuse photon density wave measurements. The wavelength of the single-mode laser was tunable from 770 nm to 802 nm (model TC40, SDL Inc., San Jose, CA). The laser diodes operated at 786 nm and 830 nm (manufactured by Sharp and Hitachi respectively). The DPDW modulation frequency was 70 MHz. All three lasers were multiplexed into nine optical fibres in the probe as light sources.

Two sets of four avalanche photodiodes were employed for detection of diffuse light at four positions, one set for the diffuse photon density wave and another set for the diffuse correlation measurement. The amplitudes and phases of the DPDW were measured for each

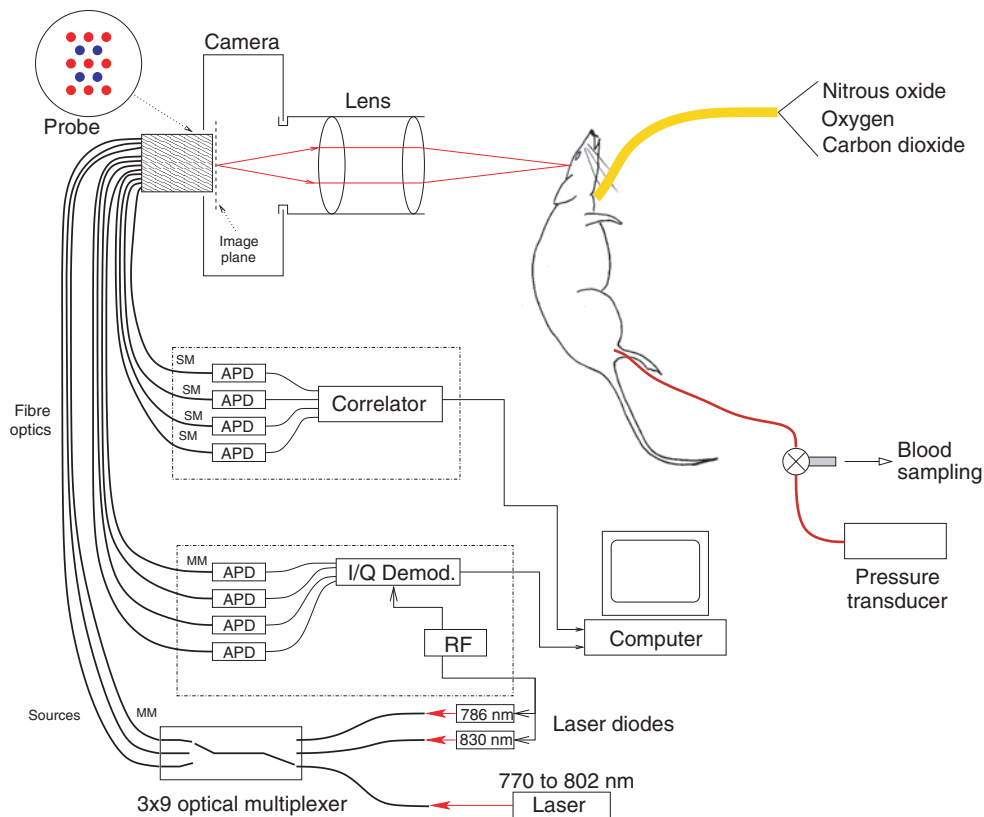


**Figure 1.** A schematic diagram of the experiment. Key: avalanche photodiode (APD), radiofrequency generator (RF), multimode fibre (MM), single-mode fibre (SM), *I/Q* demodulation (*I/Q* Demod.).

source–detector pair. For diffuse correlation flowmetry, signals from the photodiodes were directed to a correlator chip (Correlator.com, Bridgewater, NJ). The correlator chip computed the temporal intensity autocorrelation functions. A relay lens projecting the probe onto the measuring sample permitted non-contact measurements. The source and detector optical fibres were arranged in a two-dimensional pattern as shown in the upper left corner of the figure. With this design, we can reconstruct low-resolution images of the dynamics and the optical properties from the measurements. The optical multiplexer was controlled remotely by a computer.

Both the DPDW and diffuse correlation measurements take about the same amount of time, and are operated in a time-shared manner with the DPDW measurements interlaced between successive diffuse correlation measurements. A combined measurement can be made in 1 min at the fastest frame rate. The data presented in this paper were made at about 2.5 min per combined measurement.

The instrument was tested in tissue phantoms. In one important validation study we measured the diffusion coefficient of an aqueous scattering medium as a function of fluid viscosity while holding the optical properties constant. A 1% Liposine<sup>3</sup> suspension with a small

<sup>3</sup> Liposine<sup>®</sup> III 30% is manufactured by Abbott Laboratories, North Chicago, IL.

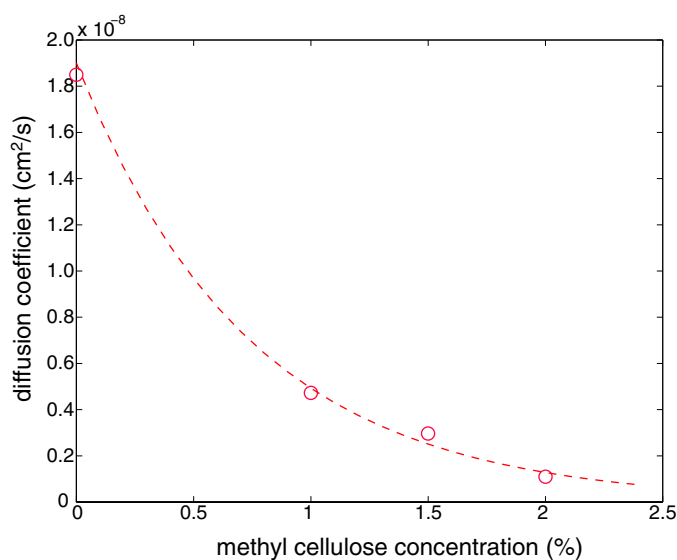


**Figure 2.** A plot of the diffusion coefficient measured by the correlation method against the concentration of methyl cellulose, a thickening agent. The error bars are about the same size as the symbols.

amount of methyl cellulose was used for these studies. Methyl cellulose is a water-soluble polymer that increases the viscosity of the solution exponentially. The reduced scattering coefficient  $\mu'_s$  of the 1% Liposine solution was determined to be approximately  $9 \text{ cm}^{-1}$  at 780 nm. Figure 2 shows the diffusion coefficient as a function of the concentration of methyl cellulose. The broken curve is an exponential fit to the data points.

#### 4. Experiment

The experiments were undertaken on adult male Sprague–Dawley rats weighing 300–325 g. Prior to the experiments the rats were fasted overnight. The animals were anesthetized with halothane (1 to 1.5%), in a mixture of 70% nitrous oxide and 30% oxygen. A catheter was placed into the femoral artery to monitor the arterial blood pressure and heart rate, and to facilitate blood sampling. A second catheter was inserted into the femoral vein for drug delivery. The body temperature was maintained at  $37^\circ\text{C}$  using a temperature controlled heating pad. After the animal was tracheotomized, it was put on a mechanical ventilator (Harvard Apparatus, South Natick, MA) and the head was fixed on a stereotaxic frame. The scalp was reflected since the fur introduced a slight distortion onto the near-infrared signals. Following the surgical procedures, halothane was withdrawn and anaesthesia was maintained with  $\alpha$ -chloralose ( $60 \text{ mg kg}^{-1}$ ), followed by supplemental doses of  $30 \text{ mg kg}^{-1}$  every hour. Blood pressure was monitored continuously and recorded on a polygraph (Grass Instruments, model 7, Quincy, MA) throughout the experiment. Arterial carbon dioxide tension was elevated by adding carbon dioxide to the breathing mixture.

When the arterial pressure had stabilized, baseline optical measurements were obtained. Carbon dioxide (6–9%) was then introduced into the breathing mixture. Measurements were made for 10 to 15 min while the animal was hypercapnic, and for 10 more minutes after the carbon dioxide was switched off. Figure 3 shows the per cent increase of  $\alpha D_B$  from the

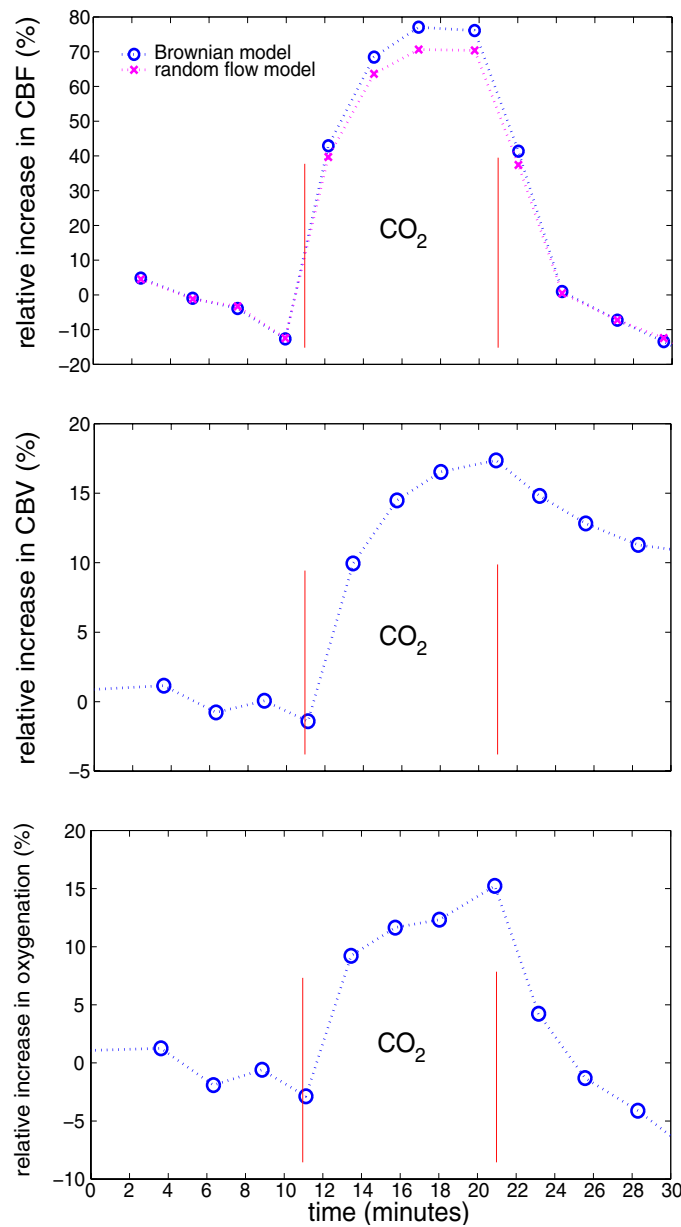


**Figure 3.** The relative increase of various measured quantities in a rat brain during carbon dioxide stimulation. Top: the diffusion coefficient (circles) or the root mean squared velocity (crosses). Middle: the tissue haemoglobin concentration. Bottom: the haemoglobin oxygen saturation. Carbon dioxide was inhaled during the time interval between the two vertical lines in the figures.

baseline level in one experiment where the animal breathed 9% CO<sub>2</sub> for 10 min. In this study the carbon dioxide partial pressure of arterial blood (*Pa*CO<sub>2</sub>) increased from 38 mm Hg to 75 mm Hg. The numbers shown in the figure were averaged over the area of the brain imaged, which comprised roughly 96 mm<sup>2</sup> of cortex. The average relative increase in  $\alpha D_B$  was about

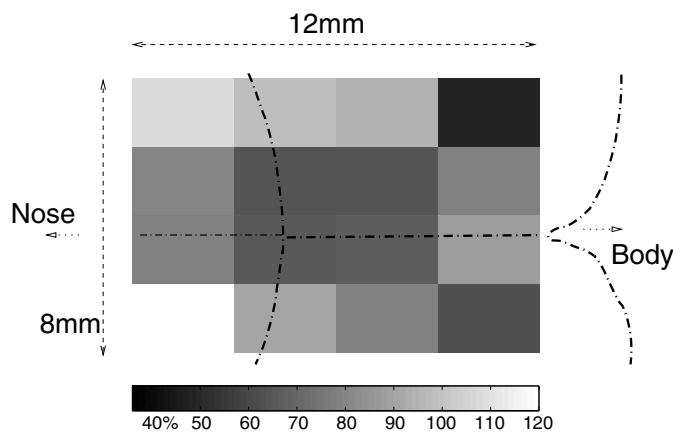
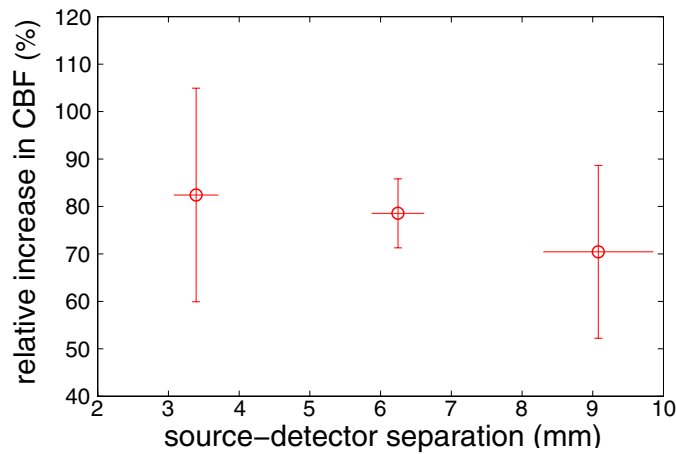


**Figure 4.** A spatial map showing the relative increase of CBF in different areas on the cortex. The numbers on the grey scale are per centage increases. The bottom photograph shows an exposed skull of a rat.

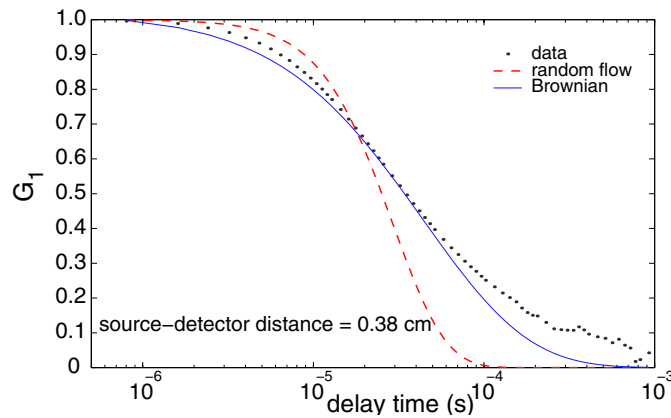
0.77 (77%) from the baseline. As discussed in the next section, this finding is consistent with other observations in the literature on the per cent increase of cerebral blood flow.

Figure 3 also shows the concurrent changes in the haemoglobin concentration as measured by NIR absorption spectroscopy averaged over the same cortical area during hypercapnia. A 0.17 (17%) increase in the haemoglobin concentration was observed. The haemoglobin concentration appears to increase at a slower rate than  $\alpha D_B$  and also decays slower after the  $\text{CO}_2$  was switched off. The average relative increase of the haemoglobin oxygenation in the cortex during the same  $\text{CO}_2$  stimulation is shown in the bottom graph of figure 3. The increase was about 16%, with the oxygenation dynamics following the flow changes more closely than the total haemoglobin concentration.

We examined the spatial homogeneity of the relative increase of CBF during hypercapnia. In particular, we plotted the 16 measurements with the shortest source–detector separation on a spatial map. These measurements were made 8 min after the start of the carbon dioxide inhalation. Figure 4 shows a low-resolution tiling of the 16 measurements. There is a considerable variance, ranging from 0.5 to 1.4 with a standard deviation of 0.19. Since the measurement depth of diffuse light techniques is roughly proportional to the spatial separation between the source and the detector, we were able to coarsely examine the depth profile of these haemodynamic changes. Figure 5 shows the average relative increase of CBF plotted against the source–detector separation. We expect that the first source–detector separation (3.3 mm)



**Figure 5.** The average relative increase of CBF due to carbon dioxide inhalation plotted as a function of the source-detector separation.



**Figure 6.** A typical  $G_1(\tau)$  measured in a normocapnic rat brain fitted by the Brownian diffusion model (full curve) and the random flow model (broken curve).  $G_1(\tau = 0)$  is normalized to unity.

derives its signal primarily from the cortical region (1.5–2.0 mm below the skull surface). In contrast, at the largest separation (9.1 mm) the signals are sensitive to white matter vascular responses. There was a  $82 \pm 22\%$  increase in CBF in the grey matter during hypercapnia, and a  $70 \pm 19\%$  increase in the white matter. Although the sensitivities of the grey matter and white matter to hypercapnia appear to be the same, the error bars are rather large. In future work we will use a layered flow model to better established the depth dependence of CBF.

**5. Discussion**

We have shown that diffuse NIR absorption spectroscopy and diffuse correlation flowmetry may be combined to enhance transcranial measurements of the vascular dynamics deep in a rat brain. The instrument probes red blood cell concentration and flow.

As we have discussed, there are two simple models which one can use to fit the measured intensity autocorrelation functions. Figure 6 shows a typical measurement of  $G_1(\tau)$  in a rat

brain in a normocapnic rest state. We have fit the data points using both the random flow model and the Brownian diffusion model. The random flow model yields a value of  $0.08 \text{ cm s}^{-1}$  for  $\sqrt{\alpha \langle V^2 \rangle}$ ; assuming  $\alpha \approx 0.1$ , then  $\sqrt{\langle V^2 \rangle}$  (the root mean squared velocity) is about  $0.25 \text{ cm s}^{-1}$ . This is a reasonable value for the speed of blood cells averaged over the arterioles, capillaries and venules in a rat brain (Seki *et al* 1996, Rosenblum 1996). However, it is also clear from figure 6 that the diffusion model fits the data better than the random flow model. We suspect that this may be due to the tortuous nature of the capillary bed, and to the peculiarities of a pulsatile complex fluid flow. Whatever the origin, we have analysed the correlation measurements using the Brownian diffusion model. This model provided good analytical fits, and effectively yielded a decay time (or a reciprocal decay rate) whose variation could be readily followed.

Experimentally we observed a 77% increase in CBF when arterial blood  $P\text{aCO}_2$  was raised from 38 mm Hg to 75 mm Hg with a concurrent increase in haemoglobin concentration of approximately 17%. The relative increase of CBF appeared to be transversely heterogeneous over the cortex (figure 4). Nevertheless, the (averaged) relative increases in grey matter and white matter behaved similarly. The response of CBF to hypercapnia has been measured by other techniques to range from 2.0 to 3.6% per mm Hg increase of  $P\text{aCO}_2$  (Fabricius and Lauritzen 1994, Wang *et al* 1995, Fabricius *et al* 1996, Forbes *et al* 1997). We have measured the response to be 2.1% per mm Hg, within the range.

The measured increase in haemoglobin concentration is smaller than the values reported by Barfod *et al* (1997); they reported an almost 40% increase in the microvascular blood cell concentration during comparable hypercapnia (from 39 to 66 mm Hg). Their study, however, was done with the skull removed. In a study using confocal microscopy, Villringer *et al* (1994) reported a 6% increase in the capillary diameter when  $P\text{aCO}_2$  was increased from 33 to 50 mm Hg, equivalent to a 12% increase in the cerebral blood volume (CBV). Grubb *et al* (1974) measured the relationship between changes in CBV and CBF during hypercapnia in rhesus monkeys; our observations of CBF and CBV changes are comparable with their observations.

Even with a low temporal resolution, we were still able to deduce from figure 3 that, in this particular animal, CBF increased more rapidly than both the haemoglobin concentration and the blood oxygenation following changes in  $P\text{aCO}_2$ . By fitting the rising portion of the data (in figure 3) to single exponential functions, we observed the rate of increase of CBF during carbon dioxide inhalation was about 50% faster than that of CBV. This is by no means a general biological conclusion on rat brain haemodynamics; more experiments need to be done to arrive at a general physiological result. Nevertheless, our observations are consistent with work by Barfod *et al* (1997) who found that the speed of the blood cell starts to increase 30 s before the blood cell concentration increases. Our scanning experiments do not as yet have the temporal resolution needed to confirm the 30 s time lag between CBF and haemoglobin concentration. Further work is under way to understand these potential discrepancies.

Our combined measurements offer us the possibility to quantitatively verify that CBF and blood oxygenation changes are self-consistent. We can use a simplified model for oxygen metabolism to relate the two measurements. We assume that the product of the difference in oxyhaemoglobin concentration between the artery perfusing the tissue and the vein draining the tissue and blood perfusion rate (in units of  $\text{ml s}^{-1}$ ) equals the oxygen consumption rate. If the metabolic rate remains unchanged during hypercapnia (Kety and Schmidt 1948), then the relative changes in CBF and haemoglobin oxygen saturation may be explicitly related, i.e.

$$\Delta[\text{HbO}] \cdot \mathcal{F} = \text{constant} \quad (8)$$

where  $\mathcal{F}$  is the blood perfusion rate, and  $\Delta[\text{HbO}]$  is the difference in oxyhaemoglobin concentration between the 'feeding' artery and the 'draining' vein. The haemoglobin oxygen

saturation  $Y$  is defined as:

$$Y = \frac{[\text{HbO}]}{[\text{HbO}] + [\text{HbR}]} \quad (9)$$

where  $[\text{HbR}]$  is the deoxyhaemoglobin concentration.  $\Delta[\text{HbO}]$  is therefore proportional to  $(Y_{\text{arterial}} - Y_{\text{venous}})$ , assuming that the total haemoglobin concentration is constant across the capillaries. The haemoglobin oxygen saturation that we measure is a weighted average of  $Y_{\text{arterial}}$  and  $Y_{\text{venous}}$ . We let  $\bar{Y} = (1 - \gamma)Y_{\text{arterial}} + \gamma Y_{\text{venous}}$  where  $\gamma$  is an arbitrary number between zero and unity. Then

$$\Delta[\text{HbO}] \propto Y_{\text{arterial}} - Y_{\text{venous}} = \frac{1}{\gamma}(Y_{\text{arterial}} - \bar{Y}). \quad (10)$$

The experimental value of  $Y_{\text{arterial}}$  was about 0.98 and is nearly constant. Substituting equation (10) into equation (8), we have

$$\begin{aligned} (0.98 - \bar{Y}(t))\mathcal{F}(t) &= (0.98 - \bar{Y}(0))\mathcal{F}(0) \\ \bar{Y}(t) &= 0.98 - (0.98 - \bar{Y}(0))\frac{\mathcal{F}(0)}{\mathcal{F}(t)}. \end{aligned} \quad (11)$$

We note that there are many models for cerebral oxygen delivery (for example Hyder *et al* 1998), and our model, which results in equation (11) relating blood perfusion and tissue haemoglobin oxygen saturation, is rather simple by comparison. Nevertheless, it permits quantitation using the measurements we have taken. The tissue blood saturation normally lies between 0.6 and 0.8 (Levy *et al* 1995). We assume that  $\bar{Y}$ (normocapnic) = 0.7 and substitute in our measured change in blood perfusion rate, i.e.

$$\mathcal{F}(\text{normocapnic})/\mathcal{F}(\text{hypercapnic}) = 1/1.77$$

then  $\bar{Y}$ (hypercapnic) = 0.823 or  $\bar{Y}$ (hypercapnic)/ $\bar{Y}$ (normocapnic) = 1.18, quite close to the measured value of 1.16. This analysis gives a sense of the new level of quantitation that the diffuse light instrument will provide in future studies.

## 6. Conclusion

We have demonstrated the ability to concurrently measure relative changes in cerebral blood flow, haemoglobin concentration and haemoglobin oxygenation with a single non-contact, non-invasive instrument. Although our pilot measurements are preliminary, results from a rat hypercapnia model are in reasonable agreement with the data from the literature, and offer the possibility for further growth and quantitation. The optical techniques used in this study are attractive also, because they enable us to measure the vascular response of deep tissues. We anticipate that the instrument will facilitate other protocols such as hypoxia and haemodilution that affect whole-brain haemodynamics. Finally, the new instrument and concept may be applicable to human studies especially in infants and neonates (see Villringer and Chance (1997), Danen *et al* (1998), and Benaron *et al* (2000) for examples of human brain measurement using NIR spectroscopy).

## Acknowledgments

This work is supported by the National Institutes of Health under grant number HL57835-01. We thank B Chance, A Villringer and R Cheung for helpful comments and discussions. Technical assistance from R Choe, T Durduran and L Zubkov is also gratefully acknowledged.

## References

- Barfod C, Akgoren N, Fabricius M, Dirnagl U and Lauritzen M 1997 Laser-Doppler measurements of concentration and velocity of moving blood cells in rat cerebral circulation *Acta Physiol. Scand.* **160** 123–32
- Benaron D A, Hintz S R, Villringer A, Boas D, Kleinschmidt A, Frahm J, Hirth C, Obrig H, van Houten J C, Kermit E L, Cheong W F and Stevenson D K 2000 Noninvasive functional imaging of human brain using light *J. Cereb. Blood Flow Metabol.* **20** 469–77
- Berne B J and Pecora R 1976 *Dynamic Light Scattering* (New York: Wiley)
- Boas D A, Campbell L E and Yodh A G 1995 Scattering and imaging with diffusing temporal field correlations *Phys. Rev. Lett.* **75** 1855–8
- Boas D A 1996 Diffuse photon probes of structural and dynamical properties of turbid media: theory and biomedical applications *PhD Dissertation* University of Pennsylvania
- Boas D A and Yodh A G 1997 Spatially varying dynamical properties of turbid media probed with diffusing temporal light correlation *J. Opt. Soc. Am. A* **14** 192–215
- Bonner R and Nossal R 1981 Model for laser Doppler measurements of blood flow in tissue *Appl. Opt.* **20** 2097
- Chance B 1989 What are the goals of magnetic resonance research? *NMR Biomed.* **2** 179–87
- Danen R M, Wang Y, Li X D, Thayer W S and Yodh A G 1998 Regional imager for low-resolution functional imaging of the brain with diffusing near-infrared light *Photochem. Photobiol.* **67** 33–40
- Dirnagl U, Niwa K, Lindauer U and Villringer A 1994 Coupling of cerebral blood flow to neuronal activation: role of adenosine and nitric oxide *Am. J. Physiol.* **267** H296–H301
- Fabricius M and Lauritzen M 1994 Examination of the role of nitric oxide for the hypercapnic rise of cerebral blood flow in rats *Am. J. Physiol.* **266** H1457–H1464
- Fabricius M, Rubin I, Bundgaard M and Lauritzen M 1996 NOs activity in brain and endothelium: relation to hypercapnic rise of cerebral blood flow in rats *Am. J. Physiol.* **271** H2035–H2044
- Forbes M L *et al* 1997 Assessment of cerebral blood flow and CO<sub>2</sub> reactivity after controlled cortical impact by perfusion magnetic resonance imaging using arterial spin-labeling in rats *J. Cereb. Blood Flow Metabol.* **17** 865–74
- Greenberg J H, Hand P J, Sylvestro A and Reivich M 1979 Localized metabolic-flow couple during functional activity *Acta Neurol. Scand.* (Suppl. 72) **60** 12–13
- Grubb Jr. R L, Raichle M E, Eichling J O and Ter-Pogossian M M 1974 The effects of changes in PaCO<sub>2</sub> on cerebral blood volume, blood flow, and vascular mean transit time *Stroke* **5** 630–9
- Hackmeier M, Skipetrov S E, Maret G and Maynard R 1997 Imaging of dynamic heterogeneities in multiple-scattering media *J. Opt. Soc. Am. A* **14** 185–91
- Haskell R C, Svaasand L O, Tsay T-T, Feng T-C, McAdams M S and Tromberg B J 1994 Boundary conditions for the diffusion equation in radiative transfer *J. Opt. Soc. Am. A* **11** 2727–41
- Hyder F, Shulman R G and Rothman D L 1998 A model for the regulation of cerebral oxygen delivery *J. Appl. Physiol.* **85** 554–64
- Kety S S and Schmidt C F 1948 The effects of altered arterial tensions of carbon dioxide and oxygen on cerebral blood flow and cerebral oxygen consumption of normal young men *J. Clin. Invest.* **27** 484–92
- Kienle A and Patterson M S 1997 Improved solutions of the steady-state and the time-resolved diffusion equations for reflectance from a semi-infinite turbid medium *J. Opt. Soc. Am. A* **14** 246–54
- Kwong K K *et al* 1992 Dynamic magnetic resonance imaging of human brain activity during primary sensory stimulation *Proc. Natl Acad. Sci. USA* **89** 5675–9
- Levy W J, Levin S and Chance B 1995 Near-infrared measurement of cerebral oxygenation: correlation with electroencephalographic ischemia during ventricular fibrillation *Anesthesiology* **83** 738–46
- Lou H C, Edvinsson L and Mackenzie E T 1987 The concept of coupling blood flow to brain function: revision required? *Ann. Neurol.* **22** 289–97
- Malonek D and Grinvald A 1996 Interactions between electrical activity and cortical microcirculation revealed by imaging spectroscopy: implications for functional brain mapping *Science* **272** 551–4
- Mandeville J B, Marota J J A, Ayata C, Zaharchuk G, Moskowitz M A, Rosen B R and Weisskoff R M 1999 Evidence of a cerebrovascular postarteriole windkessel with delayed compliance *J. Cereb. Blood Flow Metabol.* **19** 679–89
- Maret G and Wolf P E 1987 Multiple light scattering from disordered media: the effect of Brownian motion of scatterers *Z. Phys. B* **65** 409–13
- Nair P, Whalen W J and Buerk D 1975 PO<sub>2</sub> of cat cerebral cortex: response to breathing N<sub>2</sub> and 100% CO<sub>2</sub> *Microvasc. Res.* **9** 158–65
- Nossal R, Chen S H and Lai C C 1971 Use of laser scattering for quantitative determinations of bacterial motility *Opt. Commun.* **4** 35
- Phelps M E and Mazziotta J C 1985 Positron emission tomography: human brain function and biochemistry *Science* **228** 799–809

- Pine DJ, Weitz DA, Chaikin PM and Herbolzheimer E 1988 Diffusing-wave spectroscopy *Phys. Rev. Lett.* **60** 1134–7
- Rosenblum WI 1996 Conservation of flow demonstrated using the two-slit velocimeter and cross correlator in epiilluminated surface microvessels of the mouse brain *Microcirculation* **3** 187–90
- Seki J, Sasaki Y, Oyama T and Yamamoto J 1996 Fiber-optic laser-Doppler anemometer microscope applied to the cerebral microcirculation in rats *Biorheology* **33** 463–70
- Shepherd AP and Öberg P Å 1990 *Laser-Doppler Blood Flowmetry* (Boston: Kluwer)
- Villringer A, Them A, Lindauer U, Einhaupl K and Dirnagl U 1994 Capillary perfusion of the rat-brain cortex—an *in vivo* confocal microscopy study *Circ. Res.* **75** 55–62
- Villringer A and Chance B 1997 Non-invasive optical spectroscopy and imaging of human brain function *Trends Neurosci.* **20** 435–42
- Wang Q, Pelligrino DA, Baughman VL, Koenig HM and Albrecht RF 1995 The role of neuronal nitric oxide synthase in regulation of cerebral blood flow in normocapnia and hypercapnia in rats *J. Cereb. Blood Flow Metabol.* **15** 774–8
- Wilson DF, Gomi S, Pastuszko A and Greenberg JH 1993 Microvascular damage in the cortex of cat brain from middle cerebral-artery occlusion and reperfusion *J. Appl. Physiol.* **74** 580–9
- Yodh AG and Chance B 1995 Spectroscopy and imaging with diffusing light *Phys. Today* **48** 34–40
- Zijlstra WG, Buursma A and Meeuwse van der Roest WP 1991 Absorption-spectra of human fetal and adult oxyhemoglobin, deoxyhemoglobin, carboxyhemoglobin, and methemoglobin *Clin. Chem.* **37** 1633–8